An analytical six-dimensional potential energy surface for dissociation of molecular hydrogen on Cu(100).

Wiesenekker, G.; Kroes, G.J.; Baerends, E.J.

published in
Journal of Chemical Physics
1996

DOI (link to publisher)
10.1063/1.471402

document version
Publisher's PDF, also known as Version of record

An analytical six-dimensional potential energy surface for dissociation of molecular hydrogen on Cu(100)

G. Wiesenekker, G. J. Kroes, and E. J. Baerends
Theoretische Chemie, Vrije Universiteit, De Boelelaan 1083, 1081 HV Amsterdam, The Netherlands

(Received 25 October 1995; accepted 31 January 1996)

A six-dimensional (6D) potential energy surface (PES) describing the molecule–surface interaction in the dissociative chemisorption system H_2+Cu(100) is presented. The PES is based on slab calculations performed using the generalized gradient approximation (GGA) of density functional theory (DFT). To allow the use of the PES in dynamics calculations which can test the validity of the DFT/slab approach by comparing with available experiments on dissociative chemisorption, the PES was fit to an analytical form. The fit used describes the orientational dependence of the molecule–surface interaction above the high symmetry sites upto second order in spherical harmonics. The barriers to dissociation calculated for H_2 approaching with its molecular axis parallel to the surface are all located in the exit channel. Also, for different impact sites and orientations, the height and the distance to the surface associated with the barrier correlate well with the chemisorption energy of the H-atoms in the sites to which dissociation takes place; the lowest barrier (0.48 eV) is found for dissociation over the bridge site into the hollow sites, the atomic chemisorption energy being highest in the hollow sites. © *1996 American Institute of Physics.* [S0021-9606(96)03017-X]

I. INTRODUCTION

The dissociation of molecular hydrogen on copper surfaces has been well studied, both from an experimental[1–12] and theoretical[13–51] point of view. A thorough analysis of the experimental results has been presented by Michelsen and Auerbach.[52] The dissociation is translationally activated, and is enhanced by vibrational excitation of the incoming hydrogen molecule. The reactivity of the incoming molecule is also influenced by its initial rotational state.[8,12]

In performing dynamics calculations modeling the dissociation of hydrogen on copper, usually two approximations are made; it is assumed that nonadiabatic effects (for instance electron–hole pair excitations) are unimportant,[53] and that the motion of the surface atoms can be neglected.[22,23,28] Within the Born–Oppenheimer approximation, reaction probabilities are then calculated in two steps. First, a potential energy surface (PES) is constructed describing the interaction of the molecule with a static surface as a function of (ideally) all six molecular degrees of freedom. Next, a dynamics calculation is performed using the calculated PES as input. The accuracy of the calculated reaction probabilities depends first and foremost on the accuracy of the PES used, but also on whether and which approximations are introduced in the dynamics calculations.

The dynamics calculations that have been performed so far have played an important role in explaining, if not predicting, some of the experimental results. For instance, dynamics calculations[34,35,40] that used a PES based on a small cluster calculation[37] found vibrational enhancement of the reactivity before this could be confirmed conclusively in experiments using seeded molecular beams.[4,5] On the other hand, a dynamics calculation which reproduces all experimental information for the reaction on a low index copper surface has yet to appear, and to perform such a calculation remains a considerable challenge.

As noted before, inaccuracies in calculated reaction probabilities can be due to approximations made in the dynamics calculations. Early quantum dynamics calculations[31,32,34,35] employed a two-dimensional model, only treating the hydrogen–hydrogen and the molecule–surface distance as dynamical degrees of freedom. Over the last few years, the number of molecular coordinates that were modeled as fully dynamical variables in treating the H_2+Cu system was gradually increased to three[13,14,17,20,31] and four.[15,21,27,45] Full six-dimensional calculations could only be done within a classical[24,25] or mixed quantum-classical approximation.[29] Broadly speaking, a general conclusion from the higher dimensional calculations is that in principle all six molecular degrees of freedom should be treated as dynamical variables.

The other factor which has limited the accuracy of dynamics calculations in the past is the quality of the potential energy surface. The accuracy of the PES calculations depends on the way in which the metal surface is represented and on the method used to calculate the energy.

Early dynamics calculations used PES's based on cluster calculations.[37,44] In cluster calculations the surface is represented by a finite cluster of substrate atoms. In a simple cluster calculation the accuracy of the calculated binding energy depends on the size of the cluster, and in a typical series of cluster calculations the size of the cluster is increased by adding substrate atoms until the binding energy is converged with respect to the cluster size. However, for adsorbates on metallic surfaces the binding energy shows poor convergence with the size of the clusters,[54] making it difficult to reach convergence.

Later dynamics calculations used PES's based on slab

 0021-9606/96/104(18)/7344/15/$10.00

calculations.[27,50,51,55,56] In slab calculations the surface is represented by a finite number of (laterally infinite) layers of substrate atoms. The molecule is adsorbed to the slab in a periodic overlayer. The slab may be expected to describe the metallic properties of the surface fairly well. In a typical slab calculation the binding energy of a single molecule to the metal surface is obtained by increasing the number of layers in the slab and reducing the coverage until the binding energy is converged. Contrary to cluster calculations, it is relatively easy to obtain stable chemisorption energies, since the binding energy converges rapidly with respect to the number of layers and the coverage. For CO on Cu(100),[57] H on Cu(111),[55,56] and H_2 on Cu(100) (Refs. 50,51) converged results were already obtained using two layer slabs and coverages of 1/4.

In slab calculations the binding energies are usually calculated with density functional theory (DFT) using the local density approximation (LDA) and/or the generalized gradient approximation (GGA). For gas phase molecular systems it has been found that binding energies calculated using the LDA are often too high. The GGA corrects for this overbinding, often giving results close to experimental values.[58] Recently it has been shown that it is also important to use the GGA in chemisorption systems. For molecular chemisorption [CO on Pd(110) (Ref. 59) and CO on Cu(100) (Ref. 57)], the chemisorption energies calculated using the LDA are too high and are in much better agreement with experiment using the GGA. For dissociative chemisorption [H_2 on Al(110),[60,61] H_2 on Cu(111) (Ref. 33)], it has been found that reaction barriers calculated using the LDA are too low. The GGA yields reaction barriers which appear to be accurate. For H_2 on Cu(100) (Refs. 48–51) the LDA even gives a qualitatively wrong result; the 2D PES for dissociation over a bridge site into neighboring hollow sites shows no reaction barrier, which would lead to an experimentally unobserved nonzero dissociation probability for zero translational energy. The GGA yields a barrier of 0.5 eV.[50,51]

The purpose of the present work is to present a six-dimensional (6D) PES that describes the dissociative chemisorption of H_2 on Cu(100). For this purpose, DFT calculations are performed within the GGA/slab approach. To allow the use of the PES in subsequent dynamics calculations, the computed results are fit to an appropriate analytical form.

We expect that the 6D PES will be useful for two purposes. First, a 6D dynamics calculation based on the PES should allow an accurate comparison with experiment, allowing an assessment of the accuracy of the DFT method employing the GGA/slab approach. Ideally the calculation should be fully quantal and involve no dynamical approximations. Six-dimensional quantal calculations have already been performed for the H_2+OH gas-phase reaction[62,63] and for nonactivated dissociative chemisorption of H_2 on Pd(100).[64] We expect that such a calculation will soon become possible also for activated chemisorption. Second, once this calculation becomes available, the PES will also be useful for benchmark purposes, that is dynamical approximations can then be tested against fully quantal calculations employing a realistic potential energy surface.

We also present fits of two different four-dimensional (4D) PES's. One surface also depends on the coordinates for parallel translation in addition to the molecule–surface distance and the intramolecular distance, allowing an investigation of the effect of parallel translational motion on the dissociation. The orientation of the molecule is kept fixed in the calculation of this surface. The other 4D PES considers the molecule surface interaction for a fixed impact site (the bridge site, which has the lowest associated barrier) allowing an investigation of rotational effects. The construction of the 4D PES's further serves to illustrate how the 6D surface is put together.

The present work is an extension of previous work on H_2+Cu(100),[50,51] in which a two-dimensional model was used to study dissociation for a favorable impact site and orientation. We are presently performing 4D and 6D dynamics calculations based on the 4D and 6D PES's presented here. Upon publication, subroutines incorporating the 4D and 6D PES's will also be made available to others on request.

A brief outline of this paper is as follows: in Sec. II we give some details of the DFT calculations. Results obtained for reaction barriers and their locations are given for different impact sites and orientations. We also compare to results obtained by White *et al.*[48,49] for the same system using a similar method. In Sec. III the DFT results are fitted to 4D and 6D analytical forms according to constraints also discussed in that section. Section IV presents conclusions.

II. ELECTRONIC STRUCTURE CALCULATIONS

A. Method

The GGA 2D PES's were calculated using BAND,[65] a program for solving the Kohn–Sham equations of DFT (Ref. 66) for periodic systems. The program uses accurate numerical integration methods for integrals in real space[67] and in **k** space.[68] There is considerable flexibility in the description of the one-electron states; the basis sets consist of numerical atomic orbitals (NAO's), Slater type orbitals (STO's) or a combination of both. The core-electrons can be modeled using the frozen core approximation, thus avoiding any arbitrariness that may be associated with the use of pseudopotentials. The GGA Becke and Perdew corrections to the binding energies[69,70] are calculated from the self-consistent LDA Vosko–Wilk–Nusair densities.[71] This is a very good approximation to calculating the GGA energies from the self-consistent GGA density.[33] We have checked whether the DFT results are sensitive to using a different GGA (the one due to Perdew and Wang[72]) and found that this GGA yields results which are very similar (the LDA+Becke and Perdew results and the LDA+Perdew and Wang results for the barrier heights agree to within 0.1 eV).

In the calculations a two-layer slab was used to represent the Cu surface. Previous calculations on CO+Cu(100) (Ref. 57) and H_2+ Cu(100) (Refs. 50,51) have shown that adsorbate–metal interaction energies are converged to within 0.1 eV using two layers. The lattice constant was fixed at the experimental value of 4.822 a_0. A (2×2) overlayer of hydrogen molecules was used. For both parallel and tilted ap-

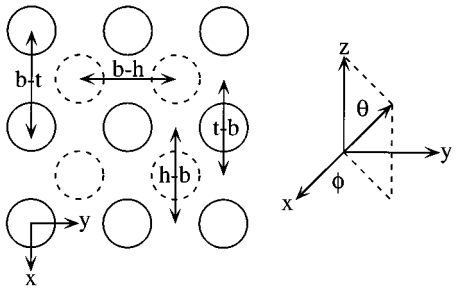

FIG. 1. Plane view of a two-layer Cu-slab, showing the Cu-atoms in the first layer (solid circles) and the second layer (dashed circles). The arrows indicate some of the dissociation paths calculated. $t-b$ means that the center of mass of the hydrogen molecule approaches a top (t) site, and that the hydrogen atoms dissociate into bridge (b) sites. Likewise $b-h$ means that dissociation takes place over a bridge site into hollow sites, etc.

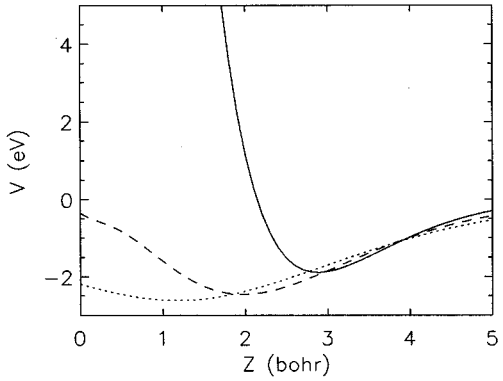

FIG. 2. The potentials for H interacting with the top site (drawn line), bridge site (dashed line), and hollow site (dotted line) are shown as functions of the molecule–surface distance.

proaches the irreducible wedge of the first Brillouin zone consists of two triangles. In each triangle six **k** points were chosen so that the analytic quadratic method for numerical integration in **k** space could be used,[68] giving a total of nine symmetry unique **k** points.

Regarding the atomic basis, the Cu atoms in the first layer have a frozen core up to $3p$, and those in the second layer up to $3d$. The basis set consists of one NAO and one STO for all valence functions (H $1s$, Cu $3d$ and $4s$) and additional $2p$ and $4p$ polarization functions on the H and Cu atoms, respectively (for further details, see Table I of Ref. 50). The NAO's and the frozen cores are obtained from a fully numerical Herman–Skillmann[73] type of calculation on the free H and Cu atoms. Convergence tests which employed a three layer slab and a (3×2) unit cell and which probed the barrier region of the PES showed that the results of the calculations using the two layer slab and a (2×2) unit cell are converged to within better than 0.1 eV. Results of additional tests which check convergence with respect to for instance the atomic basis set were presented in Ref. 50. On the basis of the tests performed, we expect that the DFT results are converged to within approximately 0.1 eV with respect to the parameters which are input to the calculations.

As explained in Sec. III, the calculation of eight 2D PES's was necessary to obtain a 6D PES in analytical form. The 2D PES's can be specified by the location of the center of mass of the hydrogen molecule (the top, bridge or hollow site), the orientation angle θ of the hydrogen molecule [parallel to the surface ($\theta=90°$) or tilted ($\theta=140.8°$)], and the site that the hydrogen atoms approach upon dissociation, or, alternatively, the angle of orientation ϕ. Some of the dissociation paths are shown in Fig. 1. Note that the values we use for θ (90° and 140.8°) correspond to two of the three zeros of $P_3(\cos\theta)$.

Each 2D PES was constructed by calculating the energy (per unit cell) of a (2×2) overlayer of H_2 molecules adsorbed to a two layer Cu slab for a number of values of Z (the distance of the center of mass of the H_2 molecule to the top layer of the slab) and r (the H–H distance). The zero of energy is defined by the sum of the energies of the two free H atoms and the energy (per unit cell) of the bare Cu slab. Five values of Z and six values of r were used, giving a grid consisting of 30 points. Using the coarse grid, the approximate locations of the saddle point were obtained. Next, to localize the saddle points more accurately, additional points were calculated in the vicinity of the approximate saddle points. All points were then fitted to the 2D analytical forms described in Sec. III, and barrier heights and locations were obtained from the analytical 2D PES's.

B. Results

1. Dissociation limits

In the entrance channel (for large Z) the interaction of the H_2 molecule with the Cu(100) surface is negligible, so the 2D PES's describe the potential energy of an isolated H_2 molecule.

For the (2×2) coverage employed in the calculations of the 2D PES's, we have shown before that the binding energies are converged with respect to the coverage for H–H distances up to 4.0 a_0, meaning that correct results are obtained for the entrance channel and the reaction zone.[50,51] For H–H distances greater than 4.0 a_0 however the interaction between the H_2 molecules in the (2×2) overlayer becomes appreciable, because the distance between the H atoms of neighboring H_2 molecules becomes similar to the H–H distance, and the calculated 2D PES's could be in error by 0.1–0.2 eV for H–H distances greater than 4.0 a_0.[50,51] To avoid this problem and also to impose the correct dissociation limit on the fitted PES's, calculations employing a lower coverage were performed to obtain accurate H atom–surface potentials. For convergence it was necessary to use a (2×2) overlayer of H atoms.[55,56] Fitted potential energy curves for the interaction of atomic H with the top, bridge and hollow sites of Cu(100) are shown in Fig. 2.

The GGA dissociation energy D_e of the free H_2 molecule is -4.83 eV. From the calculated potential curve for free H_2, a value of -4.57 eV was obtained for D_0, in good agreement with the experimental value of -4.48 eV.[74] If the H_2 molecule dissociates into hollow sites, twice the binding energy of a H atom adsorbed to a hollow site (-2.62 eV) is

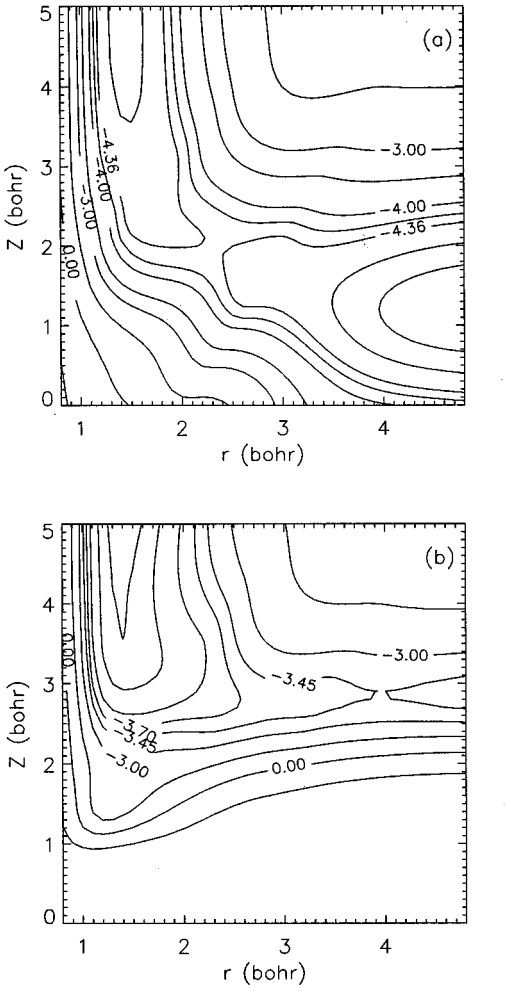

FIG. 3. Contour plots showing 2D potential energy surfaces for H_2 dissociating above the bridge site into (a) hollow sites and (b) top sites. The energies shown in the plot are in eV. In the calculations, the molecular axis was kept parallel to the surface.

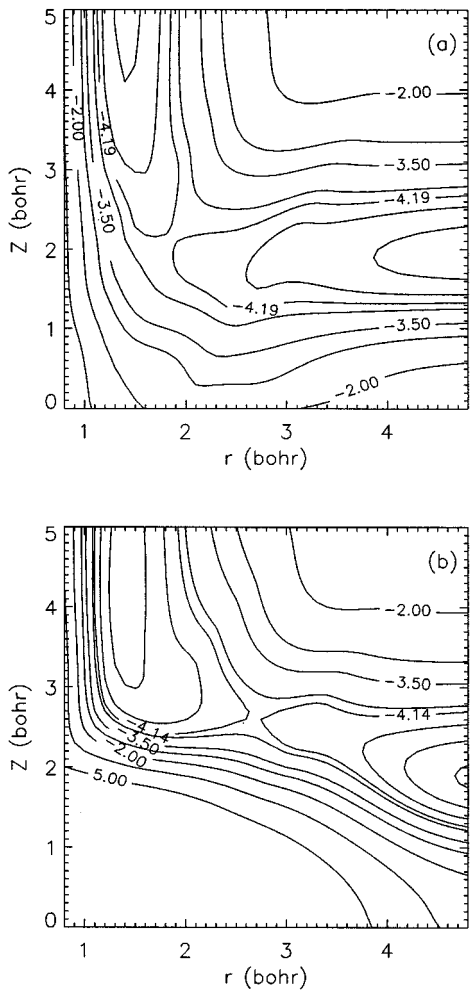

FIG. 4. Contour plots showing 2D potential energy surfaces for H_2 dissociating (a) above the hollow site into bridge sites and (b) above the top site dissociating into bridge sites. The energies shown in the plot are in eV. In the calculations, the molecular axis was kept parallel to the surface.

recovered, so dissociation into hollow sites is exothermic by 0.41 eV. Dissociation onto bridge sites is slightly exothermic by 0.11 eV. Dissociation onto top sites however is endothermic by 1.05 eV.

For the tilted approaches ($\theta = 140.8°$) only one H atom dissociates into the slab upon dissociation, so the dissociation will be endothermic for all these approaches.

2. Potential energy surfaces: Parallel orientations

The PES for dissociation over a bridge site into neighboring hollow sites [Fig. 3(a)] shows the lowest barrier to dissociation of the calculated PES's. The barrier is located in the exit channel at $r_b = 2.33\ a_0$ and $Z_b = 1.99\ a_0$. The barrier height E_b is 0.48 eV. For large values of r the PES shows the potential energy of H atoms adsorbed on hollow sites, with a minimum at $Z = 1.18\ a_0$.

The PES for dissociation over a bridge site onto neighboring top sites [Fig. 3(b)] differs markedly from the PES for dissociation into neighboring hollow sites. It shows the highest ($E_b = 1.37$ eV) and the latest ($r_b = 3.95\ a_0$) barrier to dissociation of the calculated PES's. Since the barrier height for dissociation over a bridge site onto top sites is so much larger than for dissociation into neighboring hollow sites, in-plane (helicopter) rotations are strongly hindered for dissociation over a bridge site.

The barrier heights for the PES's for dissociation over a hollow or top site into bridge sites [Figs. 4(a) and 4(b)] are comparable ($E_b = 0.64$ eV for hollow to bridge and $E_b = 0.70$ for top to bridge), but the barrier for top to bridge dissociation is later ($r_b = 2.70\ a_0$ for top to bridge, $r_b = 1.86\ a_0$ for hollow to bridge).

The heights and locations of the barriers calculated for parallel approaches are summarized in Table I. As was seen also for H_2+Cu(111), the barrier height correlates well with the variation of the chemisorption energy over the unit cell. The lowest barrier is found for dissociation over bridge sites into hollow sites (exothermic by 0.41 eV), and the highest barrier is found for dissociation over the bridge sites onto top sites (endothermic by 1.05 eV). The barriers for dissociation over top and hollow sites into bridge sites are of intermediate

TABLE I. Barrier heights (eV) and locations in r and Z (a_0) are given, for H_2 dissociating with its molecular axis kept parallel to the surface. The numbers in parentheses are the results obtained by White *et al.* (Ref. 49).

Site	Dissociation to	Barrier height	r	Z
bridge	hollow	0.48 (0.93)	2.33	1.99 (2.04)
bridge	top	1.37[a]	3.95	2.86
hollow	bridge	0.64	1.86	2.15
top	bridge	0.70 (1.21)	2.70	2.62 (2.65)

[a]Dissociation to top sites is endothermic.

heights, the dissociation being almost thermoneutral. The location of the barriers in Z also correlates well with the variation of the H atom–surface equilibrium distance. Such a correlation is expected if the barriers are located in the exit channel.[33]

Barrier heights and locations have also been calculated for the same system and using a similar method by White *et al.*[48,49] who have given explicit results for two dissociation geometries (the results given in parentheses in Table I). As can be seen from this table, our calculations are in approximate agreement with those of White *et al.* for the location of the barrier in Z. However, their barrier heights are too large compared to our results by about 0.5 eV. For reasons detailed below, we think that our results are more accurate.

First, the surface coverage ($\sqrt{2}\times\sqrt{2}$) employed by White *et al.* was probably too high. We calculate for a $\sqrt{2}\times\sqrt{2}$ coverage a barrier of 0.66 eV, compared to 0.48 eV for the (2×2) coverage. Second, in the integration over k-space we employ more points in the irreducible wedge (9) than White *et al.* (4), and the method we use to perform the k-integration (the analytic quadratic method[68]) should be more accurate. White *et al.* use a different GGA (the GGA due to Perdew and Wang[72]), but, as was already pointed out above, this GGA and the GGA we use (of Becke[69] and Perdew[70]) yield very similar barrier heights (differences are less than 0.1 eV). Finally, the calculations also differ in the atomic basis set used (White *et al.* use plane waves, we use STO's and NAO's), and in the method to represent the core electrons (White *et al.* use pseudopotentials, we use a frozen core). While it is harder to compare the calculations on these points, we note that convergence with respect to parameters characterizing the core electrons can be tested more rigorously in our approach (by varying the size of the cores), and that rigorous tests of convergence with respect to the atomic basis set have in fact been carried out.[50] Summarizing, our calculations should be somewhat better on at least two counts (size of unit cell and k-space integration). We note that more recent calculations by Kratzer *et al.*[75] which used a method which is very similar to that of White *et al.* (plane wave basis, pseudopotentials, Perdew–Wang GGA) but employed the same unit cell (2×2) and more k points in the irreducible wedge (six points) put the barrier height for bridge to hollow dissociation at 0.6 eV, which is in much better agreement with our result (0.48 eV) (Kratzer *et al.* do not give results for the other impact sites studied here).

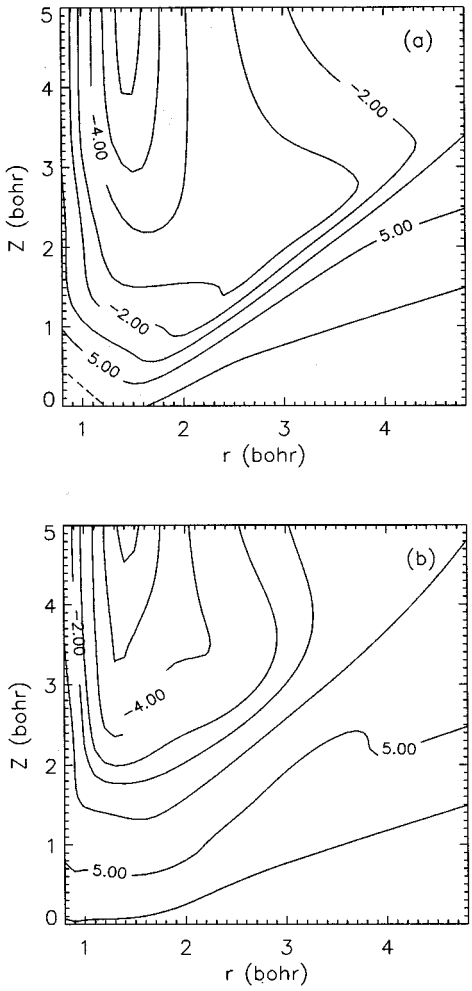

FIG. 5. Contour plots showing 2D potential energy surfaces for H_2 dissociating above the bridge site into (a) hollow sites and (b) top sites. The energies shown in the plot are in eV. The angle between the surface normal and the molecular axis is $\theta=140.8°$.

3. Potential energy surfaces: Tilted orientations

Two typical PES's for tilted approaches are shown in Fig. 5. None of the PES's for the tilted approaches show a chemisorption well. The PES's are dominated by repulsive walls for small values of Z. The origin for these walls is the repulsive interaction (for small values of Z) between a copper atom in the top layer of the slab and the H atom that dissociates into the slab. For larger values of r the repulsion starts to build up for larger values of Z, so the repulsive walls are sloping upward in Fig. 5.

In conclusion, the PES's show that the Cu(100) surface is highly corrugated towards the incoming hydrogen molecule. Both the height of the barrier (the so-called energetic corrugation) and the location of the barrier (the so-called geometric corrugation) vary over the unit cell.

III. FITTING PROCEDURE

A major goal of the present work is to obtain an analytical form of a 6D potential describing dissociative chemisorp-

tion of H_2 on Cu(100) which is based on DFT calculations. At present the DFT calculations are still quite expensive, which puts constraints on the number of different molecular orientations and projections of the molecule's position on the surface unit cell for which the electronic structure calculations can be performed. As a result, the 6D potential fitted in this section necessarily presents a compromise between feasibility and accuracy.

The potential we calculate here fulfills what we perceive to be a minimum requirement on accuracy and ability to describe six-dimensional effects. This requirement is that the potential should describe the orientational dependence of the molecule–surface interaction on the high symmetry sites (top, hollow and bridge) in an expansion of spherical harmonics including terms up to second order. As we will show below, only seven terms are required in an expansion of the potential in symmetrized rotation-diffraction functions.

We expect the resulting expansion to be quite accurate in the entrance channel and fairly accurate in the reaction zone. On the other hand, it should be inaccurate in the exit channel especially for the region of configuration space in which the H–H distance is large, the molecule–surface distance is small, and the H_2 orientation is tilted such that one atom points into the surface. In dynamics calculations that will be based on this work, the goal will be to obtain reaction probabilities and vibrational excitation probabilities which are selective with respect to the initial rovibrational state of the molecule only. These probabilities are highly averaged quantities, and we do not expect these quantities to be very dependent on the (small) inaccuracies of the potential expansion in the reaction zone. Furthermore, these probabilities should not be affected by inaccuracies in the potential expansion in the exit channel, provided that the dissociating molecule can find a low energy path towards full dissociation once the potential barrier has been crossed, such that no post-barrier reflection takes place. This is a basic assumption underlying our present work.

The six-dimensional potential is obtained in a two-stage process. First, two-dimensional potentials were calculated as functions of r and Z for two different orientations (θ=90° and 140.8°) of H_2 with the center of mass of the molecule located above either the top or the hollow site, and for four different orientations of H_2 (θ=90° and 140.8°, ϕ=0° and 90°) above the twofold bridge site, yielding eight two-dimensional potential energy surfaces. There is some arbitrariness associated with the choice of the azimuthal angle of orientation ϕ in describing dissociation above the fourfold top and hollow sites; in the present work we chose the angle ϕ to correspond to the shortest dissociation route, which is to the bridge sites in both cases (ϕ=0° rather than 45°). For dissociation above the bridge site, the angles ϕ=0° and 90° describe dissociation to either hollow sites or bridge sites, depending on which of the two bridge sites is considered in the surface unit cell. In the first stage of the fitting procedure, each two-dimensional potential is fitted individually. The expressions used are highly flexible and bear a close analogy to expressions used in fitting potentials of triatomic molecules,[76] allowing for high accuracy. In contrast, the much used LEPS form[77] is somewhat unflexible because it contains only a few adjustable parameters. An alternative method for fitting two-dimensional potential energy surfaces is described in Ref. 21. A description of the procedure used here and of the 2D PES's thus obtained is given in Sec. III A.

In the second stage, potential energy surfaces of higher dimensionality are obtained by solving sets of linear equations. This way, a 4D potential is obtained describing the orientational dependence of dissociation above the bridge site (Sec. III B), and another 4D potential is obtained describing the dependence of dissociation of H_2 kept parallel to the surface on the diffractive degrees of freedom, i.e., the coordinates X and Y defining the projection of the molecule's center-of-mass on the surface unit cell (Sec. III C). The 6D potential is obtained as described in Sec. III D. Future extensions to this potential are briefly considered in Sec. III E.

A. Two-dimensional potential energy surfaces

The expressions used in fitting the 2D PES's differ according to whether the molecular axis of H_2 is parallel to the surface (θ=90°) or tilted (θ=140.8°). For both values of θ, four 2D PES's were calculated, one describing dissociation above the top site to bridge sites, one dissociation above the hollow site to bridge sites, and two surfaces describing dissociation above the bridge site, in one case leading to dissociation to the hollow sites, and leading to dissociation to top sites in the other case. The method used to fit the four PES's with θ=90° is essentially the same as the method we used before[50,51] to fit the two-dimensional PES for dissociation above the bridge site into hollow sites. For completeness, we give a shorter description below. For a more detailed explanation, the reader is referred to Refs. 50,51.

The reader should note that the 2D PES's (and therefore also the 4D and 6D potentials derived later on in this work) do not contain physisorption wells, for two reasons. First, with the use of the GGA density functional theory is not expected to yield good results for van der Waals interactions, though results should be good for the chemical wells and for the barrier to reaction. Secondly, the physisorption well depth (≈30 meV) resulting from detailed experiments[78–80] on low energy scattering of H_2 from Cu(100) is smaller than the lowest barrier for dissociation (0.48 eV, see Sec. III B 2) by more than an order of magnitude. It should therefore be safe to neglect the physisorption well in scattering calculations which aim at obtaining reaction probabilities or vibrational excitation probabilities (the threshold for vibrational excitation of H_2 is approximately 0.5 eV). It is for these purposes that we have constructed the potential energy surfaces presented in this work.

1. Parallel orientations

To obtain accurate 2D fits for dissociation geometries with θ=90°, we start with a ''two-body potential'' which is quantitatively correct in the entrance channel, and also in the exit channel for r equal to the Cu–Cu distance, where the dissociated atoms are above the site to which dissociation

proceeds. We make sure that the two-body potential is qualitatively similar to the full DFT potential in the reaction zone by shifting from a two-body expression which is appropriate to the entrance channel to one which is appropriate to the exit channel. For the purpose of defining the reaction zone, we first define a new two-dimensional coordinate system, which is trivially related to the r,Z system (for how we take the r and Z axes, see Fig. 3). The new system is a system of polar coordinates R,ζ which has its origin at the point $(r_{\rm ref},Z_{\rm ref})$, where R is the distance to the origin. The angle ζ is the angle made with the r-axis by the line passing through the origin $(r_{\rm ref},Z_{\rm ref})$ and the point (r,Z) now being described by (R,ζ) (see also Fig. 5 of Ref. 50). In the new coordinate system, the reaction zone is a region lying to the left of and below the origin [$(r_{\rm ref},Z_{\rm ref})$, $r_{\rm ref}$ and $Z_{\rm ref}$ are taken as suitably large numbers]. The reaction zone is further enclosed by two lines which make angles $\zeta=\zeta_0-\Delta\zeta$ and $\zeta=\zeta_0+\Delta\zeta$ with the r-axis (see also Fig. 5 of Ref. 50). Angles $\zeta<\zeta_0-\Delta\zeta$ correspond to the entrance channel, and angles $\zeta>\zeta_0+\Delta\zeta$ to the exit channel. The expression used for the two-body potential is

$$V_{2b}=V_{2b}^{A}(r,Z), \quad \zeta<\zeta_0-\Delta\zeta, \tag{1a}$$

$$V_{2b}=f_c(\zeta)V_{2b}^{A}(r,Z)+[1-f_c(\zeta)]V_{2b}^{B}(r,Z), \quad \zeta_0-\Delta\zeta\leqslant\zeta\leqslant\zeta_0+\Delta\zeta, \tag{1b}$$

$$V_{2b}=V_{2b}^{B}(r,Z), \quad \zeta>\zeta_0+\Delta\zeta, \tag{1c}$$

where the switching function $f_c(\zeta)$ is defined by

$$f_c(\zeta)=\frac{1}{2}+\frac{1}{2}\cos(\chi), \tag{2a}$$

$$\chi=\frac{[\zeta-(\zeta_0-\Delta\zeta)]\pi}{2\Delta\zeta}, \tag{2b}$$

ζ being defined by

$$\zeta=\tan^{-1}\frac{(Z-Z_{\rm ref})}{(r-r_{\rm ref})}. \tag{2c}$$

The parameters $Z_{\rm ref}$ and $r_{\rm ref}$ are taken as large positive numbers ($Z_{\rm ref}=18.3\ a_0$ and $r_{\rm ref}=11.0\ a_0$) to allow the switching to be performed without singularities resulting in the energy-accessible coordinate region. The values used for ζ_0 and $\Delta\zeta$ are 61.5° and 2.5°, respectively. The values of the parameters ζ_0 and $\Delta\zeta$, $r_{\rm ref}$ and $Z_{\rm ref}$ were chosen to accurately describe the location of the reaction region (which should of course enclose the barrier to reaction or the saddle-point) for the three 2D surfaces which are most important for dissociation (top to bridge, hollow to bridge, and bridge to hollow, $\theta=90°$). In conjunction with the appropriate forms of $V_{2b}^{A}(r,Z)$ and $V_{2b}^{B}(r,Z)$ discussed below, the shifting procedure outlined above produces a two-body potential which is already qualitatively correct in its appearance, in that it produces an energy diagram in which the entrance and exit channels are separated by a reaction region, in which the saddle point is located.[37] Note that the shifting procedure used here and below for the three-body potential (see below) ensures the continuity of the potential and its first derivatives with respect to r and Z (V_{2b}, $dV_{2b}/d\zeta$, and dV_{2b}/dR are continuous also for $\zeta=\zeta_0-\Delta\zeta$ and $\zeta=\zeta_0+\Delta\zeta$, and the same will be true for the three-body potential discussed below). Because the potentials and its first derivatives with respect to r and Z (alternatively, the forces along r and Z) are continuous, our 2D potentials (and also the 4D and 6D potentials we will construct below) can also be used with the classical trajectory method.[81]

TABLE II. Fitting coefficients for attractive two-body potentials. For the meaning of the parameters, see the text.

Parameter	H_2	Cu–H Hollow	Top	Bridge
D_e(eV)	4.8286	2.6200	1.8885	2.4669
$x_e(a_0)$[a]	1.40	1.18	2.83	1.98
$a_1(a_0^{-1})$	2.282	1.200	1.202	1.490
$a_2(a_0^{-2})$	1.555	0.5756	−0.3681	0.7676
$a_3(a_0^{-3})$	0.7533	0.1109	−0.1619(−1)[b]	0.1354
$a_4(a_0^{-1})$	2.23	1.20	1.10	1.50

[a] x_e is r_e for H_2, and Z_e for Cu–H.
[b] The notation (−1) means 10^{-1}.

In the entrance channel (region A, reactants) we have the H_2 molecule experiencing a repulsive interaction with the surface, and the potential is given approximately by

$$V_{2b}^{A}(r,Z)=V_{\rm att}(r)+V_{\rm rep}(Z). \tag{3}$$

Here, we take the GGA bare H_2 potential as $V_{\rm att}(r)$ and fit it to a modified Rydberg form,

$$V_{\rm att}=-D_e(1.0+a_1\rho+a_2\rho^2+a_3\rho^3)\exp(-a_4\rho), \tag{4a}$$

where $\rho=r-r_e$. The constants obtained for the fit are the same as used previously and are collected in Table II for completeness. The Pauli repulsion was taken as

$$V_{\rm rep}=a\ \exp[-bZ], \tag{4b}$$

with the a and b constants taken as before (see Table III).

In the exit channel, with r equal to the surface lattice constant ($4.822\ a_0$) we have the H-atoms experiencing an attractive interaction with the surface, while being repelled from one another, and the potential is written

$$V_{2b}^{B}(r,Z)=2V_{\rm att}(Z)+V_{\rm rep}(r). \tag{5}$$

The repulsive potential $V_{\rm rep}(r)$ was taken as in Eq. (4b), with Z replaced by r (see Table III for the values used). The potential describing the chemical interaction of atomic hydrogen with the surface $[V_{\rm att}(Z)]$ was taken to be dependent on the site to which dissociation proceeds. For all high symmetry sites, density functional (GGA) results for atomic hydrogen interacting with the surface were least squares fitted

TABLE III. Fitting coefficients for repulsive two body potentials. For the meaning of the parameters, see the text.

Parameter	Cu–H_2	H–H
a(eV)	24.0	45.81
$b(a_0^{-1})$	1.39	1.365

TABLE IV. Fitting coefficients for the three-body part of the potential in the entrance channel (V^A), for H_2 oriented with its molecular axis kept parallel to the surface.

Parameter	Site dissociation to	Bridge hollow	Bridge top	Top bridge	Hollow bridge
$\gamma_1(a_0^{-1})$		1.0	1.0	0.9	1.0
$r_0(a_0)$		2.0	2.0	2.0	2.0
$\gamma_2(a_0^{-1})$		1.1	0.7	0.85	1.0
$Z_0(a_0)$		2.0	2.0	2.0	2.0
c_0(eV)		−2.1560	−2.9797	0.6958	−1.9490
c_1(eV a_0^{-1})		−2.7105	−9.2141	−1.4854	−2.5636
c_2		−1.3396	7.4464	−8.0244	−0.3308
c_{11}(eV a_0^{-2})		0.7389	−7.1154	3.4990	0.8482
c_{12}		−6.5802	13.2067	−6.0491	−4.8289
c_{22}		−0.3934	−11.0051	6.1140	−0.6152
c_{111}(eV a_0^{-3})		2.0041	1.4948	1.1502	1.8968
c_{112}		−5.2146	8.5243	−7.5985	−3.8903
c_{122}		−2.9961	−16.5798	−3.4012	−2.2264
c_{222}		−0.3158	5.6414	−2.6036	0.1154
c_{1111}(eV a_0^{-4})		0.6260	2.5960	−1.5375	0.3242
c_{1112}		1.6811	3.6896	6.4113	1.9678
c_{1122}		−5.4469	−9.8696	−4.5182	−4.7124
c_{1222}		−0.2007	6.2623	0.7283	0.4212
c_{2222}		−0.1421	−0.9143	0.3818	0.1420
c_{11112}(eV a_0^{-5})		1.8476	1.5199	7.1376	2.1009
c_{11122}		−2.5337	−3.2314	−4.5661	−2.8550
c_{11222}		0.3421	1.2001	−0.8347	0.4746
c_{12222}		−0.1529	−0.8158	−0.2140	0.1788
$r_{3b}(a_0)$		⋯	⋯	⋯	⋯
$Z_{3b}(a_0)$		⋯	⋯	−0.4	⋯

to the form Eq. (4a) with $\rho = Z - Z_e$. The resulting fit parameters are given in Table II, and the potentials are plotted in Fig. 2. As noted before, the dissociation to the hollow and bridge sites is exothermic, while dissociation to top sites is endothermic by approximately 1 eV.

In the next step, the actual fitting is done. For points lying in the entrance channel and the reaction zone, the energy differences between the GGA energy and the two-body potential are least-squares fitted to the ''three-body'' expression

$$V_{3b}^A(r,Z) = P(s_1,s_2)[1.0 - \tanh(\gamma_1 s_1) \times [1.0 - \tanh(\gamma_2 s_2)], \quad (6a)$$

$$P(s_1,s_2) = c_0 + c_1 s_1 + c_2 s_2 + c_{11} s_1^2 + c_{12} s_1 s_2 + \cdots, \quad (6b)$$

retaining all terms up to fourth order in Eq. (6b), and also some fifth order terms. In Eqs. (6), $s_1 = r - r_0$ and $s_2 = Z - Z_0$. For the coefficients thus obtained, see Table IV. For all 2D potential energy surfaces, we made sure that the fits thus obtained deviated from the density functional potential values by less than 0.1 eV for total interaction energies smaller than −2.5 eV (i.e., in the region of configuration space which is energetically accessible at scattering energies lower than 1.5 eV). An advantage of the form of Eqs. (6) is that it goes exponentially to zero for either r or Z (or both) large, allowing one to impose the correct asymptotic behavior by choosing a suitable form for the two-body potential (see above). At small values of r and or Z, the total interaction is usually dominated by the repulsion in the ''two-body'' part of the interaction, though in exceptional cases artifacts may result from extrapolation of the three-body potential to small values of r and or Z. In cases where this happened, we set $V_{3b}^A(r,Z)$ equal to $V_{3b}^A(r_{3b},Z_{3b})$ for either $r < r_{3b}$ for $Z < Z_{3b}$, or both. In all cases, we make sure that r_{3b} and Z_{3b} are taken small enough to ensure that this measure only affects the potential where it is already quite repulsive.

The same procedure is then followed for points lying in the exit and reaction zones, obtaining $V_{3b}^B(r,Z)$ (see Table V). Both $V_{3b}^A(r,Z)$ and $V_{3b}^B(r,Z)$ represent accurate fits to the GGA energy in the reaction zone, and we obtain an expression for the three-body potential which is valid in all zones using an expression which is entirely analogous to Eq. (1), but now involving the three-body potentials $V_{3b}^A(r,Z)$ and $V_{3b}^B(r,Z)$. The same values were used for the parameters Z_{ref}, r_{ref}, ζ_0, and $\Delta\zeta$ in all cases. The full potential obtained by adding the two-body and three-body expressions is plotted in Fig. 3 for dissociation above the bridge site, and in Fig. 4 for dissociation above the top and hollow sites. The heights and locations of the barriers to dissociation have already been given in Table I and discussed in Sec. II.

The approach used here to fit 2D PES's has two important advantages. First of all, the three-body expression we use is flexible enough to allow for accurate fitting. Fit errors are less than 0.1 eV for $E < -2.5$ eV, which is well above the energies classically accessible for a collision energy less than 1 eV and for H_2 initially in its $v = 0$ or $v = 1$ vibrational state. The H_2 potential minimum is at −4.83 eV, while the quantum of vibration is approximately 0.5 eV. Second, the desired asymptotic behavior is easily imposed through the

TABLE V. Fitting coefficients for the three-body part of the potential in the exit channel (V^B), for H_2 oriented with its molecular axis kept parallel to the surface.

Parameter	Site dissociation to	Bridge hollow	Bridge top	Top Bridge	Hollow bridge
$\gamma_1(a_0^{-1})$		1.0	1.0	1.0	1.3
$r_0(a_0)$		2.0	2.0	2.0	2.1
$\gamma_2(a_0^{-1})$		0.8	0.7	1.0	0.7
$Z_0(a_0)$		2.0	2.0	2.0	2.1
c_0(eV)		−2.2286	−2.9726	0.7130	−1.8948
c_1(eV a_0^{-1})		−2.5300	−7.1966	−2.2416	−2.4470
c_2		−1.1797	5.6741	−11.9575	−0.2142
c_{11}(eV a_0^{-2})		1.8106	−4.9790	3.0942	1.2522
c_{12}		−5.7072	8.9385	6.4401	−4.3031
c_{22}		0.2921	−10.4362	4.9622	−0.2519
c_{111}(eV a_0^{-3})		1.9273	−1.3116	2.9115	1.9030
c_{112}		0.1141	12.2737	−15.4768	−2.5154
c_{122}		−4.3194	−17.8690	−3.1597	−2.9563
c_{222}		0.5909	7.4498	1.2188	0.3319
c_{1111}(eV a_0^{-4})		−0.8624	1.2555	−1.6825	−0.7357
c_{1112}		3.1068	4.8007	7.5091	4.2234
c_{1122}		−0.2988	−10.2352	−6.0247	−6.0518
c_{1222}		−2.8572	9.3522	−14.8042	−0.2134
c_{2222}		0.2038	−1.4559	0.6946	0.1774
c_{11112}(eV a_0^{-5})		−0.6658	−3.6249	−0.4289	−0.4121
c_{11122}		0.9616	10.5544	3.9293	1.2341
c_{11222}		0.2364	−9.1065	4.4243	−1.7706
c_{12222}		−0.7368	−0.4598	−2.7901	0.2227
$r_{3b}(a_0)$		⋯	⋯	⋯	⋯
$Z_{3b}(a_0)$		⋯	⋯	−0.4	⋯

use of a two-body potential which employs a shifting function to ensure that, for large Z, the potential becomes the bare H_2 potential, and that, for large r, the potential becomes the potential of two chemisorbed H-atoms. The shifting procedure does have one drawback. At the border lines where it is turned on (for instance, for $\zeta=\zeta_0-\Delta\zeta$) the second and higher order derivatives of the potential with respect to r and Z are not continuous. This may lead to small artifacts, as is illustrated in Fig. 6, where we plot the potential for dissociation above the hollow site to bridge sites as a function of the reaction path coordinate s for motion along the reaction path.[82] Two small artifacts are seen in the regions where the switching function is turned on, one just before the barrier, and one after the barrier. We believe that these artifacts will not significantly affect the scattering for two reasons. First, the ''height'' that may be associated with these features is always less than the fitting error, which is less than 0.1 eV for $E<-2.5$ eV, and therefore quite small. Second, the extent over which the artifact occurs in coordinate space is somewhat less than the wavelength that may be associated with molecular and atomic motion at critical energies. For instance, the wavelength associated with molecular motion at a collision energy of 0.5 eV is 0.54 a_0, while the wavelength associated with the dissociative motion at an energy of 1.0 eV is 0.77 a_0. The extent over which the artifacts occurs is typically 0.2–0.3 a_0.

The small artifacts discussed above might have been avoided with the use of spline fits. A disadvantage of this approach would be that the resulting expression, though still analytical, would contain too many parameters to be easily communicable to other researchers. Therefore, it would be less useful for benchmark purposes. While the small artifacts might also have been avoided with the use of other fit expressions, we believe that none of the other fit methods presently in use yield the high accuracy that our expression does.

2. Tilted orientations

The GGA energies calculated for $\theta=140.8°$ were fitted in a slightly different manner, in which the accuracy requirement in the exit channel is relaxed. As was already mentioned in the introduction to this section, we do not expect the orientational dependence of the molecule–surface potential to be described accurately in the exit channel in case spherical harmonics are included up to second order only, especially in case tilted orientations are considered. By the same token, it will not be very useful to attempt producing accurate fits of the 2D potential energy surfaces calculated for $\theta=140.8°$ in the region of configuration space which is well into the exit channel. A qualitatively correct form of the potential in this region will work, provided that the assumption discussed earlier, that the molecule will find a low energy path to dissociation once it has crossed the reaction zone, is correct. In this case, in the exit channel we only need a form of the potential which emphasizes that the potential becomes increasingly repulsive for increasingly tilted orientations along a low energy path towards dissociation, which will be located close to orientations where $\theta=90°$.

The expression used to fit the PES's calculated for $\theta=140.8°$ have been chosen accordingly. For each combination of dissociation site and azimuthal angle, the potential is written as

$$V=V_{2b}(r,Z,\theta)+f_d(\xi)V_{3b}(r,Z). \tag{7}$$

In Eq. (7), the two-body potential is similar to $V_{2b}^A(r,Z)$ of Eq. (3), except that we now take $V_{\rm rep}(Z)$ to depend on θ, through

$$V_{\rm rep}=a/2\{\exp[-bZ_1]+\exp[-bZ_2]\}. \tag{8}$$

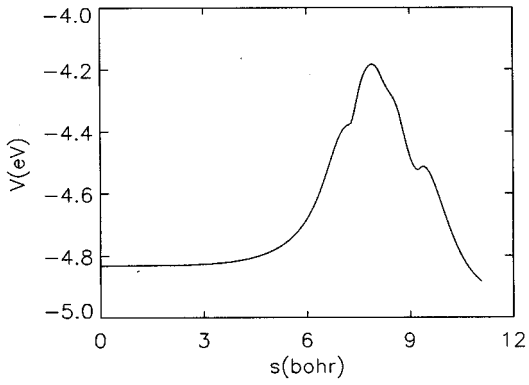

FIG. 6. The potential for dissociation above the hollow site is plotted along the reaction path as a function of the reaction path coordinate s (Ref. 82).

TABLE VI. Fitting coefficients for the three-body part of the potential, for tilted orientations of H_2 (θ=140.8°).

Parameter	Site dissociation to	Bridge hollow	Bridge top	Top bridge	Hollow bridge
$\gamma_1(a_0^{-1})$		0.7	0.9	1.1	0.5
$r_0(a_0)$		2.0	2.0	2.0	2.0
$\gamma_2(a_0^{-1})$		0.9	1.0	1.1	0.9
$Z_0(a_0)$		2.0	2.0	1.5	2.0
c_0(eV)		−2.1188	−0.3886	59.3269	−2.3219
c_1(eV a_0^{-1})		−4.0813	−1.1126	32.4383	−4.1615
c_2		0.4164	−0.7195	−77.1394	0.9462
c_{11}(eV a_0^{-2})		−3.4684	0.6899	−19.5761	−3.2764
c_{12}		0.4743	−4.0069	−7.8027	0.5885
c_{22}		−1.2139	−1.0341	51.3360	−1.2271
c_{111}(eV a_0^{-3})		−2.6264	4.8652	45.9639	−0.9752
c_{112}		1.2696	−7.6348	109.7566	1.0814
c_{122}		−2.6213	−5.0197	1.8432	−2.8336
c_{222}		0.6974	0.4707	−16.1009	0.5741
c_{1111}(eV a_0^{-4})		−1.2464	3.5126	66.6261	0.2340
c_{1112}		−0.8167	2.9013	61.0663	−0.2781
c_{1122}		−3.7379	−8.8692	−49.9826	−2.1130
c_{1222}		0.6057	−2.5059	−2.5965	−0.0139
c_{2222}		−0.3532	−0.4979	0.3488	−0.3451
c_{11112}(eV a_0^{-5})		−0.8963	7.3996	−38.0010	−1.1280
c_{11122}		−1.8449	−4.9131	−61.4955	−0.0721
c_{11222}		−0.5767	−2.6632	−15.3063	−0.1545
c_{12222}		−0.5765	−0.3286	−4.3638	−0.2424
$r_{3b}(a_0)$		⋯	0.9	⋯	⋯
$Z_{3b}(a_0)$		1.0	0.9	⋯	⋯

In Eq. (8), Z_1 and Z_2 are the Z-coordinates of the individual atoms, where the same a and b parameters are used as were used in Eq. (4b), so that Eq. (8) would reproduce Eq. (4b) for θ=90°. The region made up by the entrance and reaction zones is supposed to be separated from the exit channel by the line going through the point ($r=2\ a_0$, $Z=1\ a_0$) and making an angle of 45° with the r-axis, such that the three barriers calculated from the 2D PES's that are lower than 1 eV (see Table I) fall well into the reaction region. To define this line separating reaction and product regions for tilted orientations, we introduce a system of polar coordinates analogous to the one previously defined in Sec. III A 1, but with another origin [$(r_{\mathrm{ref2}}, Z_{\mathrm{ref2}})=(15\ a_0, 14\ a_0)$], ξ now being the polar angle. The polar angle defining this line [which passes through the origin $(r_{\mathrm{ref2}}, Z_{\mathrm{ref2}})$] is taken as $\xi=\xi_0-\Delta\xi=45°$. For points which fall into the entrance and reaction region, and also for points such that $\xi<\xi_0+\Delta\xi$, where

$$\xi=\tan^{-1}\frac{(Z-Z_{\mathrm{ref2}})}{(r-r_{\mathrm{ref2}})}, \tag{9}$$

the energy difference between the GGA energy and the two-body potential is fitted to Eqs. (6) (see Table VI). Rather than also fitting the potential in the ''far exit zone'' defined by $\xi>\xi_0+\Delta\xi$, we now simply switch off the three-body term for angles ξ lying between $\xi=\xi_0-\Delta\xi$ and $\xi=\xi_0+\Delta\xi$. The function $f_d(\xi)$ is completely analogous to the function $f_c(\zeta)$, the difference being that $f_d(\xi)$ acts as a damping function, merely switching off the three-body term. The parameters ξ_0(46.15°) and $\Delta\xi$ (1.15°) defining $f_d(\xi)$ are taken such that (i) $\xi_0-\Delta\xi=45°$, and (ii) $\Delta\xi$ is large enough to ensure that the damping of the three-body term is performed in a smooth enough manner. The two-body expression presented in Eq. (7) is used also in the exit channel, which is of course not correct in that it neglects the attractive interaction one of the H-atoms may have with the surface. However, as was stressed before the expression adopted here merely serves to emphasize that in the exit channel and along low energy paths towards dissociation the interaction becomes increasingly repulsive for increasingly tilted orientations of H_2.

Fits of the 2D PES's calculated for dissociation over the bridge site and θ=140.8° are shown in Fig. 5. The 2D PES's for dissociation above the top and hollow sites and calculated for θ=140.8° look quite similar, and are not shown here.

B. The 4D PES for dissociation over the bridge site

With fits to the four 2D PES's now being calculated for dissociation above the bridge site, we can expand the orientational dependence of the molecule–surface interaction using spherical harmonics up to order 2. The expression used is

$$\begin{aligned} V_{4\mathrm{D}}(r,Z,\theta,\phi)=&V_{00b}(r,Z)Y_{00}(\theta,\phi)\\ &+V_{20b}(r,Z)Y_{20}(\theta,\phi)\\ &+V_{2eb}(r,Z)Y_{2e}(\theta,\phi), \end{aligned} \tag{10}$$

where Y_{00} and Y_{20} are the usual spherical harmonics (see Ref. 83), and $Y_{2e}(\theta,\phi)$ is related to such functions by

$$Y_{2e}(\theta,\phi)=\sqrt{\frac{1}{2}}\,[Y_{22}(\theta,\phi)+Y_{2-2}(\theta,\phi)]. \tag{11}$$

Equation (10) contains three r,Z dependent expansion coefficients, while four 2D PES's are available, leaving some arbitrariness in the choice of how the expansion coefficients are obtained. This arbitrariness is resolved by demanding that (i) the 4D expression reproduce the two 2D PES's for dissociation to hollow sites and dissociation to top sites which were calculated for $\theta=90°$, and that (ii) the average of the 4D expression over ϕ reproduce the average of the two 2D PES's calculated for $\theta=140.8°$. The expansion coefficients can then be obtained from the fitted 2D PES's using

$$V_{20b}=\frac{1}{2}\,[V_{bh140}+V_{bt140}-V_{bh90}-V_{bt90}]/$$
$$[Y_{20}(\theta=140.8°)-Y_{20}(\theta=90°)], \tag{12}$$

$$V_{00b}=\frac{1}{2}\,[V_{bh90}+V_{bt90}-V_{20b}Y_{20}(\theta=90°)]/Y_{00}, \tag{13}$$

and

$$V_{2eb}=\frac{1}{2}\,[V_{bh90}-V_{bt90}]/Y_{2e}(\theta=90°,\phi=0°). \tag{14}$$

In Eqs. (12)–(14), the fits to the two-dimensional PES's are designated by a subscript of which the first index denotes the site above which dissociation takes place (b for bridge), the second index denotes the site towards which the atoms dissociate (h for hollow and t for top), and the rest of the subscript denotes the angle θ. In writing Eq. (14), $\phi=0$ corresponds to dissociation to hollow sites. Note that, through our choice of the values of θ for which 2D potentials were calculated, using Eqs. (12) and (13) to obtain the ϕ-independent expansion functions is formally equivalent to using three point Gauss–Legendre quadrature to obtain these expansion functions from the ϕ-averaged potentials for θ equal to the zeros of $P_3(\cos\theta)$. Also note that, in order to avoid artefacts resulting from extrapolating V to large values of θ ($>140.8°$), we impose a maximum of one hartree on the 2D potentials used to obtain the expansion coefficients. It should be emphasized that this procedure affects the potential only well into the classically forbidden region and in the far exit zone.

Together with the fit expressions given in Sec. III A, Eqs. (12)–(14) define an analytical expression for a 4D potential describing the orientational dependence of dissociation over the bridge site. A nice feature of the expansion is that, with the use of the close-coupling wave packet method,[84] the potential coupling matrix obtained from our potential is real symmetric. This can be seen quite easily. If we choose to expand the potential in Y_{lm} functions only, we will have $V_{22}=V_{2-2}=\sqrt{\frac{1}{2}}V_{2e}$, such that both V_{22} and V_{2-2} are real. Likewise, V_{00} and V_{20} are real. Any potential matrix element can be written as a sum of products involving the expansion functions V_{00}, V_{20}, V_{22}, and V_{2-2} on the one hand, and integrals over three spherical harmonics on the other hand. Because the latter are real per definition and because the expansion functions are real for the present model, the potential coupling matrix is real symmetric.

Concerning the quality of the fit, we first consider parallel orientations. Note that the fit accurately describes the DFT results for $\theta=90°$ and $\phi=0°$ (bridge to hollow) and $\theta=90°$ and $\phi=90°$ (bridge to top). This is because the procedure used to generate the 4D potential is such that the 4D potential simply interpolates between the DFT results for these two orientations. As a result, for these orientations the error in the fit is as small as the error in the fits of the 2D surfaces (less than 0.1 eV for all points on the surface which are energetically accessible in dissociative chemisorption experiments). Because we do not include information concerning intermediate values of ϕ, for intermediate values of ϕ the potential is expected to be somewhat less accurate, especially in the exit zone.

We next consider the quality of the fit for tilted orientations, focusing on the reaction zone. We recall that the procedure used to obtain the 4D potential was such that for $\theta=140.8°$ the average of the 4D fit to the results for $\phi=0°$ and $\phi=90°$ reproduces the average of those results. We may then obtain a measure of the quality of the 4D fit in the reaction zone by comparing results of using the fit for $\phi=0°$ and $\phi=90°$ with the actual results for these angles rather than their averages. For $\phi=0°$ (bridge to hollow dissociation), the calculated 2D fit for $r=Z=2\ a_0$ predicts a potential energy of -3.60 eV, while the 4D fit yields -3.10 eV. For $\phi=90°$ (bridge to top dissociation) and the same values of r and Z, the 2D potential predicts an energy of -1.87 eV, while the 4D potential is now 0.50 eV too low (-2.37 eV). For intermediate values of ϕ ($0°\leqslant\phi\leqslant90°$), the error is probably not larger than the errors obtained for $\phi=0°$ and $\phi=90°$. In the reaction zone, the potentials at $\phi=0°$ and $\phi=90°$ represent extremes, the potential being large at $\phi=90°$ and small at $\phi=0°$. The fitting procedure used is such that the variation of the potential with ϕ is less than it should be, i.e., the fit underestimates the potential at 90° and overestimates it at 0°.

For $\theta=140.8°$, in the entrance channel, the 4D potential does a much better job at reproducing the ϕ-dependence of the calculated 2D fits, the agreement being typically of the order of 0.05 eV or less for values of $r\leqslant2\ a_0$. Errors are expected to be larger in the exit zone, as is discussed at the beginning of this section.

Concerning intermediate values of θ, we expect our PES to be most accurate for the values of θ which are most important for the reaction (close to 90°). The PES should be least accurate for values of $\theta\geqslant140.8°$, but these orientations are less important for the reaction. For the present, we are satisfied with the accuracy of the fit, though it will be clear that for tilted orientations the PES can be further improved in the reaction zone by performing calculations for more angles, such that Y_{lm} functions of order four can also be included in the potential expansion.

C. The 4D PES for dissociation of H_2 kept parallel to the surface

With fits to two-dimensional PES's now being calculated for dissociation above all the high symmetry sites, it is possible to expand the potential in such a way that the dependence of the potential on the diffractive degrees of freedom is correctly described on the high symmetry sites. To do so, we expand the potential in symmetry-adapted functions (adapted to the C_{4v} symmetry of the unit cell), which consist of linear combinations of plane-wave diffraction functions,[85]

$$V_{4D}(r,Z,x,y)=V_{00}(r,Z)H_{00}(x,y)+V_{10}(r,Z)H_{10}(x,y)+V_{11}(r,Z)H_{11}(x,y), \tag{15}$$

where

$$H_{00}(x,y)=\sqrt{1/A}, \tag{16}$$

$$H_{10}(x,y)=\sqrt{1/A}\{\cos Gx+\cos Gy\}, \tag{17}$$

$$H_{11}(x,y)=2\sqrt{1/A}\{\cos Gx\times\cos Gy\}, \tag{18}$$

$$G=2\pi/a_l. \tag{19}$$

In Eqs. (16)–(19), A is the surface of the surface unit cell, and a_l is the Cu–Cu distance (4.822 a_0). The expansion functions defined in Eqs. (16)–(19) are normalized on the unit cell (just like the spherical harmonics are normalized on the unit sphere), and belong to the totally symmetric A_1 representation under C_{4v}. The expansion functions can be calculated from the fitted two-dimensional PES's by solving the appropriate linear equations according to

$$V_{00}=\sqrt{A}/4\{V_{tb90}+V_{hb90}+2V_{bh90}\}, \tag{20}$$

$$V_{10}=\sqrt{A}/4\{V_{tb90}-V_{hb90}\}, \tag{21}$$

$$V_{11}=\sqrt{A}/8\{V_{tb90}+V_{hb90}-2V_{bh90}\}. \tag{22}$$

There is some arbitrariness associated with the choice of the 2D PES for dissociation above the bridge site, as we could also have selected the PES describing dissociation to top sites. We chose to use the surface for dissociation to the hollow sites as it is more likely that the molecule will follow the lower energy path to dissociation. Anyway, the purpose of the 4D PES defined through Eqs. (16)–(22) is limited in that it is to study the effect of including the diffractive degrees of freedom in model calculations on dissociative chemisorption. Combined rotation/diffraction effects can be studied using the 6D potential described below. As was done in Sec. III B, we impose a maximum of one hartree on the 2D potentials used to obtain the expansion coefficients.

The 4D potential incorporating the diffraction degrees of freedom interpolates between the 2D potentials for impacts on the high symmetry sites with θ=90° and ϕ taken such that above each high symmetry site the energetically most favorable dissociation route is described (above the top and hollow sites, the shortest dissociation routes also represent the energetically most favorable dissociation routes). As such, the potential is expected to yield a reasonable description of the X and Y dependence of the molecule–surface interaction for θ=90° and ϕ taken such that the most favorable dissociation route is obtained. With these restrictions, above the high symmetry sites the 4D potential is as accurate as the 2D potentials. It should be less accurate for values of X and Y which are intermediate, especially in the exit channel where r is large and Z is small.

D. The 6D PES

The potential expansion that describes the orientational dependence of the molecule–surface potential up to second order in spherical harmonics above the high symmetry sites, and is otherwise of minimum size, is

$$\begin{aligned}V_{6D}(r,Z,\theta,\phi,x,y)=&V_{0000}(r,Z)Y_{00}(\theta,\phi)H_{00}(x,y)\\&+V_{2000}(r,Z)Y_{20}(\theta,\phi)H_{00}(x,y)\\&+V_{0010}(r,Z)Y_{00}(\theta,\phi)H_{10}(x,y)\\&+V_{2010}(r,Z)Y_{20}(\theta,\phi)H_{10}(x,y)\\&+V_{0011}(r,Z)Y_{00}(\theta,\phi)H_{11}(x,y)\\&+V_{2011}(r,Z)Y_{20}(\theta,\phi)H_{11}(x,y)\\&+V_{2e10}(r,Z)Y_{2e}(\theta,\phi)H_{B_1 10}(x,y),\end{aligned} \tag{23}$$

with

$$H_{B_1 10}(x,y)=\sqrt{1/A}\{\cos Gx-\cos Gy\}. \tag{24}$$

Note that the rotation-diffraction functions which make up the expansion functions in Eq. (23) are all totally symmetric under C_{4v}.

The r,Z dependent expansion coefficients are calculated from the eight 2D potentials, for which analytical expressions and fitting coefficients were given in Sec. III A, in much the same way as described in Secs. III B and III C. First, above each site the potential is expanded in spherical harmonics. This way, expansion coefficients V_{00b}, V_{20b}, and V_{2eb} are obtained for the 4D potential for dissociation over the bridge site, as described in Sec. III B. Expansion coefficients V_{00t}, V_{20t} for the 3D potential describing dissociation over the top site are obtained from equations which are analogous to Eqs. (12) and (13), except that the expressions used no longer involve averages over ϕ. The same procedure is used to obtain expansion coefficients V_{00h}, V_{20h} for dissociation over the hollow site. Next, we obtain the 6D expansion coefficients using expressions which are completely analogous to Eqs. (20)–(22), but now involve coefficients for expansions in spherical harmonics, for instance,

$$V_{0000}=\sqrt{A}/4\{V_{00t}+V_{00h}+2V_{00b}\}, \tag{25}$$

$$V_{0010}=\sqrt{A}/4\{V_{00t}-V_{00h}\}, \tag{26}$$

$$V_{0011}=\sqrt{A}/8\{V_{00t}+V_{00h}-2V_{00b}\}, \tag{27}$$

and similarly for the expansion coefficients related to the Y_{20} spherical harmonic. The coefficient V_{2e10} is obtained from

$$V_{2e10}=\sqrt{A}/2\ V_{2eb}. \tag{28}$$

As was done in the previous sections, we impose a maximum of one hartree on the 2D potentials used to obtain the expansion coefficients. We emphasize again that this procedure, while avoiding artifacts, only affects the potential expansion at points (r,Z) which are either classically forbidden for all dissociation sites and orientations or are well into the exit zone. We also emphasize that the 6D potential we introduce here is fully analytical, because the (r,Z) dependent expansion coefficients that form part of the expression for the 6D potential [Eq. (23)] are obtained from analytical expressions relating 2D potentials which are available in analytical form (Sec. III A).

Regarding the accuracy of the 6D potential, we may say the following. The 6D potential exactly interpolates the four 2D fits to the potentials describing top to bridge, hollow to bridge, bridge to hollow, and bridge to top dissociation, for parallel orientations (θ=90°). These 2D fits are quite accurate (maximum errors less than 0.1 eV in the energetically accessible region). Likewise, for tilted orientations (θ =140.8°) the 6D potential interpolates the two 2D fits describing dissociation above the top and hollow sites, and it should be quite accurate above these sites in both the entrance zone and the reaction zone. Above the bridge site, the 6D potential is exactly equal to the 4D potential described in Sec. III B, and for its accuracy for tilted orientations we refer to the discussion in that section. Quite generally, we can say that the 6D potential will be least accurate for combinations of values of θ, ϕ, X, and Y which can be said to be furthest away from the values of θ, ϕ, X, and Y for which the 2D potentials were calculated. Deviations from actual DFT results are expected to be smallest in the entrance zone and greatest in the exit zone, and should be greater for tilted orientations than for parallel orientations. We have already stressed that the present 6D potential of necessity represents a compromise between accuracy and feasibility (see the introduction to the present section). Nevertheless, we intend to improve it in the future, and some possible ways to do this are discussed below in Sec. III E.

E. Future extensions

The expansion we use for the 6D potential [Eq. (23)] may be seen as a ''minimum size'' expression consistently defining a 6D potential. There are obvious ways of improving it by including extra terms. The present form does not describe the dependence on ϕ for dissociation over the top and hollow sites, and as such does not distinguish between for instance dissociation above the top site to the hollow sites and dissociation above the top site to the bridge sites. Describing the dependence on ϕ above the fourfold hollow and top sites becomes possible if the expansion is enlarged to contain also spherical harmonics of order 4. Furthermore, increasing the expansion in this way should have the added advantage that the orientation dependence above the bridge site should be described more accurately in the reaction zone also for $\theta \geqslant 140.8°$.

It may well be that it should be even more important to also focus on describing the orientational dependence of the potential above sites in the unit cell which are of lower symmetry. For instance, we might also require that our potential should contain expansion functions such that (i) all diffraction functions with $m \leqslant n \leqslant 1$ are present (n and m are the usual diffraction labels); (ii) all second order spherical harmonics are present. In this case, the added expansion functions would be (for details see Ref. 85)

$$g_{21E10}(x,y,\theta,\phi) = \sqrt{2/A}\,\sin Gx Y_{21e}(\theta,\phi) + \sqrt{2/A}\,\sin Gy Y_{21o}(\theta,\phi), \tag{29}$$

$$g_{21E11}(x,y,\theta,\phi) = \sqrt{4/A}\,\sin Gx\,\cos Gy Y_{21e}(\theta,\phi) + \sqrt{4/A}\,\cos Gx\,\sin Gy Y_{21o}(\theta,\phi), \tag{30}$$

$$g_{22B_211}(x,y,\theta,\phi) = \sqrt{4/A}\,\sin Gx\,\sin Gy Y_{22o}(\theta,\phi), \tag{31}$$

where

$$Y_{21e}(\theta,\phi) = \sqrt{\frac{1}{2}}\,[-Y_{21}(\theta,\phi) + Y_{2-1}(\theta,\phi)], \tag{32}$$

$$Y_{21o}(\theta,\phi) = -\frac{1}{i}\,\sqrt{\frac{1}{2}}\,[Y_{21}(\theta,\phi) + Y_{2-1}(\theta,\phi)], \tag{33}$$

$$Y_{22o}(\theta,\phi) = \frac{1}{i}\,\sqrt{\frac{1}{2}}\,[Y_{22}(\theta,\phi) - Y_{2-2}(\theta,\phi)]. \tag{34}$$

While including these terms would further improve the 6D potential, it would also necessitate calculating three more 2D potential energy surfaces for judiciously chosen points (x,y,θ,ϕ). Nevertheless, including the functions of Eqs. (29)–(31) in the expansion may well be important, as these terms would contribute to changes in the magnetic quantum number m_j in collisions where the molecule is not above a high symmetry site. Changes in the magnetic quantum number allow the molecule to change its orientation while the collision takes place, which may be quite important for overcoming the barrier to reaction. Because of the possible importance of the expansion functions given in Eqs. (29)–(31), further extending our potential to also include these functions is high on our list.

In summary, in the future we hope to update our 6D potential by including more spherical harmonic and plane wave expansion terms. At present, including these terms was not possible due to the high costs of the calculations. Other improvements that will be considered is adding anisotropy to the exponential term describing the repulsion of H_2 by the surface, and adding an anisotropic van der Waals interaction term. The latter additions would make the PES also useful for studying low energy scattering, and the required parameters are available from detailed experiments.[78–80]

IV. CONCLUSIONS

We have presented a six dimensional (6D) potential energy surface (PES) describing the dissociative chemisorption

of H_2 over Cu(100). The surface is based on slab calculations performed using the generalized gradient approximation (GGA) of density functional theory (DFT).

The DFT calculations on which the PES is based are still fairly expensive, and the potential therefore represents a compromise between feasibility and accuracy. We have required that the PES describe the orientational dependence of the molecule–surface potential above the high symmetry sites in an expansion of spherical harmonics including terms up to second order. High accuracy is required in the entrance and reaction zones.

The potential expansion used contains seven terms, and the fitting was performed in a two-stage process. First, eight two-dimensional (2D) potential energy surfaces were calculated for impacts on high symmetry sites and appropriate molecular orientations. The 2D surfaces were fit using an expression which allows one to impose a suitable asymptotic behavior in the entrance and exit channels, and also allows for high accuracy. Next, the expansion coefficients for the 6D potential were obtained in such a way from the 2D fits that the 6D potential interpolates the 2D potentials for the impacts and orientations for which they were calculated.

The electronic structure calculations show a fairly high energetic and geometric corrugation in the reaction barrier for H_2 approaching with its molecular axis parallel to the surface. The barriers are of the late type, being located in the exit channel. In agreement with this, for particular impact sites there is a correlation between the barrier height and the distance of the barrier to the surface on the one hand, and the chemisorption energy of the atoms in the sites to which dissociation takes place on the other hand. The dissociation to the hollow sites is most exothermic, and we find the smallest barrier height (0.48 eV) for dissociation over the bridge site into hollow sites. The highest barrier is found for bridge to top sites, for which dissociation is endothermic. The barriers for the dissociation over the top and hollow sites into bridge sites are of intermediate height, the dissociation to the bridge sites being only slightly exothermic.

Dynamics calculations performed in the past for the H_2+Cu system indicate that in principle all six molecular degrees of freedom should be modelled as dynamical variables. Ideally, such a 6D dynamical calculation would be fully quantal. Six dimensional dynamical calculations have already been performed for the H_2+OH reaction and for the nonactivated dissociative chemisorption of H_2 on Pd(100). Therefore, such a calculation should soon become possible for activated chemisorption as well. The potential energy surface we present here can be used as input to these calculations, allowing a test of the accuracy of the DFT/slab approach used by comparing with available experiments. The 6D surface can also be used to test consequences of making various dynamical approximations in benchmark calculations.

ACKNOWLEDGMENTS

We would like to thank J. G. Snijders and R. C. Mowrey for useful discussions. This research was made possible through a grant of computertime by the Dutch National Computing Facilities foundation (NCF), and through financial support by the Royal Netherlands Academy of Arts and Sciences (KNAW). This work was supported in part by the Netherlands Foundation for Chemical Research (SON) with financial aid from the Netherlands Organization for Scientific Research (NWO).

[1] G. Anger, A. Winkler, and K. D. Rendulic, Surf. Sci. **220**, 1 (1989).
[2] D. J. Auerbach, C. T. Rettner, and H. A. Michelsen, Surf. Sci. **283**, 1 (1993).
[3] M. Balooch, M. J. Cardillo, D. R. Miller, and R. E. Stickney, Surf. Sci. **46**, 385 (1974).
[4] H. F. Berger, M. Leisch, A. Winkler, and K. D. Rendulic, Chem. Phys. **175**, 425 (1990).
[5] B. E. Hayden and C. L. A. Lamont, Phys. Rev. Lett. **63**, 1823 (1989).
[6] B. E. Hayden and C. L. A. Lamont, Surf. Sci. **243**, 31 (1991).
[7] A. Hodgson, J. Moryl, P. Traverso, and H. Zhao, Nature **356**, 501 (1992).
[8] H. A. Michelsen, C. T. Rettner, D. J. Auerbach, and R. N. Zare, J. Chem. Phys. **98**, 8294 (1993).
[9] P. B. Rasmussen, P. M. Holmblad, H. Christoffersen, P. A. Taylor, and I. Chorkendorff, Surf. Sci. **287-288**, 79 (1993).
[10] C. T. Rettner, D. J. Auerbach, and H. A. Michelsen, Phys. Rev. Lett. **68**, 1164 (1992).
[11] C. T. Rettner, D. J. Auerbach, and H. A. Michelsen, Phys. Rev. Lett. **68**, 2547 (1992).
[12] C. T. Rettner, H. A. Michelsen, and D. J. Auerbach, J. Chem. Phys. **102**, 4625 (1995).
[13] J. Dai, J. Sheng, and Z. H. Zhang, J. Chem. Phys. **101**, 1555 (1994).
[14] J. Dai and J. Z. H. Zhang, Surf. Sci. **319**, 193 (1994).
[15] J. Dai and J. Z. H. Zhang, J. Chem. Phys. **102**, 6280 (1995).
[16] G. R. Darling and S. Holloway, J. Chem. Phys. **97**, 734 (1992).
[17] G. R. Darling and S. Holloway, J. Chem. Phys. **97**, 5182 (1992).
[18] G. R. Darling and S. Holloway, Chem. Phys. Lett. **191**, 396 (1992).
[19] G. R. Darling and S. Holloway, Surf. Sci. Lett. **304**, L461 (1994).
[20] G. R. Darling and S. Holloway, Surf. Sci. **307-309**, 153 (1994).
[21] G. R. Darling and S. Holloway, J. Chem. Phys. **101**, 3268 (1994).
[22] G. R. Darling and S. Holloway, Surf. Sci. Lett. **321**, L189 (1994).
[23] G. R. Darling and S. Holloway, Surf. Sci. **336**, L771 (1995).
[24] C. Engdahl, B. I. Lundqvist, U. Nielsen, and J. K. Nørskov, Phys. Rev. B **45**, 11 362 (1992).
[25] C. Engdahl and U. Nielsen, J. Chem. Phys. **98**, 4223 (1993).
[26] C. Engdahl and B. I. Lundqvist, Chem. Phys. Lett. **215**, 103 (1993).
[27] A. Gross, B. Hammer, M. Scheffler, and W. Brenig, Phys. Rev. Lett. **73**, 3121 (1994).
[28] A. Gross, Surf. Sci. Lett. **314**, L843 (1994).
[29] A. Grüneich, A. J. Cruz, and B. Jackson, J. Chem. Phys. **98**, 5800 (1993).
[30] A. Gross, J. Chem. Phys. **102**, 5045 (1995).
[31] D. Halstead and S. Holloway, J. Chem. Phys. **88**, 7197 (1988).
[32] D. Halstead and S. Holloway, J. Chem. Phys. **93**, 2859 (1990).
[33] B. Hammer, M. Scheffler, K. W. Jacobsen, and J. K. Norskov, Phys. Rev. Lett. **73**, 1400 (1994).
[34] M. Hand and S. Holloway, J. Chem. Phys. **91**, 7209 (1989).
[35] M. R. Hand and S. Holloway, Surf. Sci. **211-212**, 940 (1989).
[36] J. Harris and A. Liebsch, Phys. Scr. **4**, 14 (1983).
[37] J. Harris and S. Andersson, Phys. Rev. Lett. **55**, 1583 (1985).
[38] J. Harris, S. Andersson, C. Holmberg, and P. Nordlander, Phys. Scr. **13**, 155 (1986).
[39] J. Harris, S. Holloway, T. S. Rahman, and K. Yang, J. Chem. Phys. **89**, 4427 (1988).
[40] J. Harris, Surf. Sci. **221**, 335 (1989).
[41] X. Jianjun, J. Ping, and Z. Kaiming, J. Phys. Condensed Matter **6**, 7217 (1994).
[42] S. Kumar and B. Jackson, J. Chem. Phys. **100**, 5956 (1994).
[43] S. Küchenhoff and W. Brenig, Surf. Sci. **258**, 302 (1991).
[44] J. E. Müller, Surf. Sci. **272**, 45 (1992).
[45] U. Nielsen, D. Halstead, S. Holloway, and J. K. Nørskov, J. Chem. Phys. **93**, 2879 (1990).
[46] J. K. Nørskov, J. Chem. Phys. **90**, 7461 (1989).
[47] J. Sheng and J. Z. H. Zhang, J. Chem. Phys. **99**, 1373 (1993).
[48] J. A. White and D. M. Bird, Chem. Phys. Lett. **213**, 422 (1993).

[49] J. A. White, D. M. Bird, M. C. Payne, and I. Stich, Phys. Rev. Lett. **73**, 1404 (1994).
[50] G. Wiesenekker, G. J. Kroes, and E. J. Baerends, J. Chem. Phys. **102**, 3873 (1995).
[51] G. Wiesenekker, G. J. Kroes, and E. J. Baerends, J. Chem. Phys. **103**, 5168 (1995).
[52] H. A. Michelsen and D. J. Auerbach, J. Chem. Phys. **94**, 7502 (1991).
[53] J. K. Nørskov, J. Vac. Sci. Technol. **18**, 421 (1981).
[54] G. te Velde and E. J. Baerends, Chem. Phys. **177**, 399 (1993).
[55] A. Forni, G. Wiesenekker, E. J. Baerends, and G. F. Tantardini, Int. J. Quantum Chem. **52**, 1067 (1994).
[56] A. Forni, G. Wiesenekker, E. J. Baerends, and G. F. Tantardini, J. Phys. Condensed Mater **7**, 7195 (1995).
[57] P. H. T. Philipsen, G. te Velde, and E. J. Baerends, Chem. Phys. Lett. **226**, 583 (1994).
[58] E. Folga and T. Ziegler, J. Am. Chem. Soc. **115**, 5169 (1993).
[59] P. Hu, D. A. King, S. Crampin, M.-H. Lee, and M. C. Payne, Chem. Phys. Lett. **230**, 501 (1994).
[60] B. Hammer, K. W. Jacobsen, and J. K. Norskov, Surf. Sci. Lett. **297**, L68 (1993).
[61] K. Gundersen, W. Jacobsen, J. K. Norskov, and B. Hammer, Surf. Sci. **304**, 131 (1994).
[62] D. H. Zhang and Z. H. Zhang, J. Chem. Phys. **101**, 1146 (1994).
[63] D. Neuhauser, J. Chem. Phys. **100**, 9272 (1994).
[64] A. Gross, S. Wilke, and M. Scheffler, Phys. Rev. Lett. **75**, 2719 (1995).
[65] G. te Velde and E. J. Baerends, Phys. Rev. B **44**, 7888 (1991).
[66] W. Kohn and L. J. Sham, Phys. Rev. A **140**, 1133 (1965).
[67] G. te Velde and E. J. Baerends, J. Comput. Phys. **99**, 84 (1992).
[68] G. Wiesenekker, G. te Velde, and E. J. Baerends, J. Phys. C **21**, 4263 (1988).
[69] A. D. Becke, Phys. Rev. A **38**, 3098 (1988).
[70] J. P. Perdew, Phys. Rev. B **33**, 8822 (1986).
[71] S. H. Vosko, L. Wilk, and M. Nusair, Can. J. Phys. **58**, 1200 (1980).
[72] J. P. Perdew, J. A. Chevary, S. Vosko, K. Jackson, M. R. Pederson, D. J. Singh, and C. Fiolhais, Phys. Rev. B **64**, 6671 (1992).
[73] F. Herman and S. Skillman, *Atomic Structure Calculations* (Prentice–Hall, Englewood Cliffs, 1963).
[74] G. Herzberg, *Molecular Spectra and Molecular Structure*, 2nd ed. (van Nostrand, New York, 1950), Vol. I.
[75] P. Kratzer, B. Hammer, and J. K. Nørskov, Surf. Sci. (submitted).
[76] K. S. Sorbie and J. N. Murrell, Mol. Phys. **29**, 1387 (1975).
[77] A. E. Depristo and A. Kara, Adv. Chem. Phys. **77**, 163 (1991).
[78] S. Andersson, L. Wilzén, and M. Persson, Phys. Rev. B **38**, 2967 (1988).
[79] S. Andersson, L. Wilzén, and M. Persson, Phys. Rev. B **40**, 8146 (1989).
[80] L. Wilzén, F. Althoff, S. Andersson, and M. Persson, Phys. Rev. B **43**, 7003 (1991).
[81] R. N. Porter and L. M. Raff, in *Dynamics of Molecular Collisions*, edited by W. H. Miller (Plenum, New York, 1976), p. 1.
[82] S. Holloway, Comments At. Mol. Phys. **27**, 335 (1992).
[83] A. Messiah, *Quantum Mechanics* (North-Holland, Amsterdam, 1991), Vol. I.
[84] R. C. Mowrey, J. Chem. Phys. **99**, 7049 (1993).
[85] G. J. Kroes, J. G. Snijders, and R. C. Mowrey, J. Chem. Phys. **102**, 5512 (1995).